ACS APPLIED MATERIALS & INTERFACES

RESEARCH ARTICLE

www.acsami.org

Effect of Surface Morphology on the Optical Properties in Metal−Dielectric−Metal Thin Film Systems

Eunice S. P. Leong, Yan Jun Liu, Bing Wang, and Jinghua Teng*

Institute of Materials Research and Engineering, Agency for Science, Technology and Research (A*STAR), 3 Research Link, Singapore 117602, Singapore

ABSTRACT: The effect of surface morphology on the optical properties in a metal−dielectric−metal (MDM) thin film was investigated. Ag films were thermally evaporated at different rates to obtain different surface roughnesses and grain sizes. The reflectance spectra of the Ag/MgF_2/Ag films show a dip due to surface-roughness-induced excitation of surface plasmon polaritons. The dip position varies from 650 to 800 nm, depending on the surface morphology of the multilayered film. An empirical relationship was found between the optical properties (i.e., the dip position and its linewidth) and the Ag film structural properties (i.e., surface roughness, grain size, and filling factor). The causes of and contributions to the shift of the dip position and the linewidth of the dip were discussed. The study is important to metal−dielectric-based structures, and the unique feature of such a MDM film could be used for color filters.

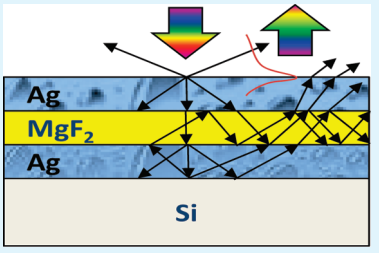

KEYWORDS: metal−dielectric−metal, surface roughness, surface plasmons, color filters, reflectance spectrum, Ag film

INTRODUCTION

Plasmonics pave the way for manipulation of optical signals at nanoscale by coupling light to coherent electronic excitations (known as surface plasmon resonances) at the interface between dielectric materials and metal nanostructures.[1] The strong confinement of light associated with surface plasmon resonances has led to the development of a toolbox of various subwavelength photonic components, such as waveguides,[2,3] switches,[4] lenses,[5−7] spacers,[8−11] and metamaterials.[12,13] In all of these applications, the metal−dielectric interface plays an extremely important role in fulfilling the desired functions. To achieve efficient coupling between light and surface plasmons (i.e., surface plasmon polaritons, SPPs), the noble-metal films are usually very thin (<100 nm). Because metals have poor affinity to substrates and grow in the Volmer−Weber mode, only semicontinuous thin films can be formed for such a thickness.[14−17] This leads to rough films with large scattering loss and, hence, additional damping, which is undesirable for plasmonic and metamaterial devices. However, the presence of surface roughness can also facilitate the excitation of SPPs.[1] Several studies have been carried out to investigate the influence of surface roughness for single metallic thin films.[1,17−21] Nevertheless, there are very few studies on this effect for metal−dielectric−metal (MDM) films, which is more important in many optical device applications.[22−27] In this paper, we choose Ag and MgF_2 to form the plasmonic MDM thin film system and investigate the effect of surface roughness on its optical properties. We give an analytical relationship between the reflectance and the Ag film structural properties based on the combined morphological and optical study. The application of such a MDM thin film system is also explored.

EXPERIMENTAL SECTION

In our experiment, a 30-nm-thick Ag film was first deposited on a large Si substrate at a rate of ~6 nm/min. Subsequently, a 30-nm-thick MgF_2 film was deposited on top of the Ag film at a rate of ~1.5 nm/min. The deposition was done in the same chamber without breaking the vacuum via an Auto306 (Edwards) thermal evaporator. The large substrate was then cleaved into six smaller pieces for thermal evaporation of the top Ag layer at different deposition rates. The thickness of the top Ag film was fixed at ~30 nm. The deposition thickness was recorded every minute, and the deposition rates were averaged to be ~0.55, 1.37, 2.42, 3.48, 5.76, and 6.8 nm/min, respectively, for the six samples.

RESULTS AND DISCUSSION

Atomic force microscopy (AFM) analysis at a scale size of 1 × 1 μm^2 was performed on multilayered films to investigate how the deposition rate affects the surface morphology. Because the bottom Ag and MgF_2 films were deposited at the same time for all samples, we assume that their surface morphologies are the same. Therefore, the results from the analysis for the different samples are only caused by the different deposition rates for the top Ag film. The histograms of the grain size and the corresponding AFM images at different deposition rates are shown in Figures 1a−1f. The formation of small grains (<25 nm) dominates at a low deposition rate of 0.55 nm/s (see Figure 1a). At faster deposition rates (1.37−3.48 nm/s), a mixture of small to large grains (>50 nm) is observed on the samples (see

Received: December 28, 2010
Accepted: March 10, 2011
Published: March 10, 2011

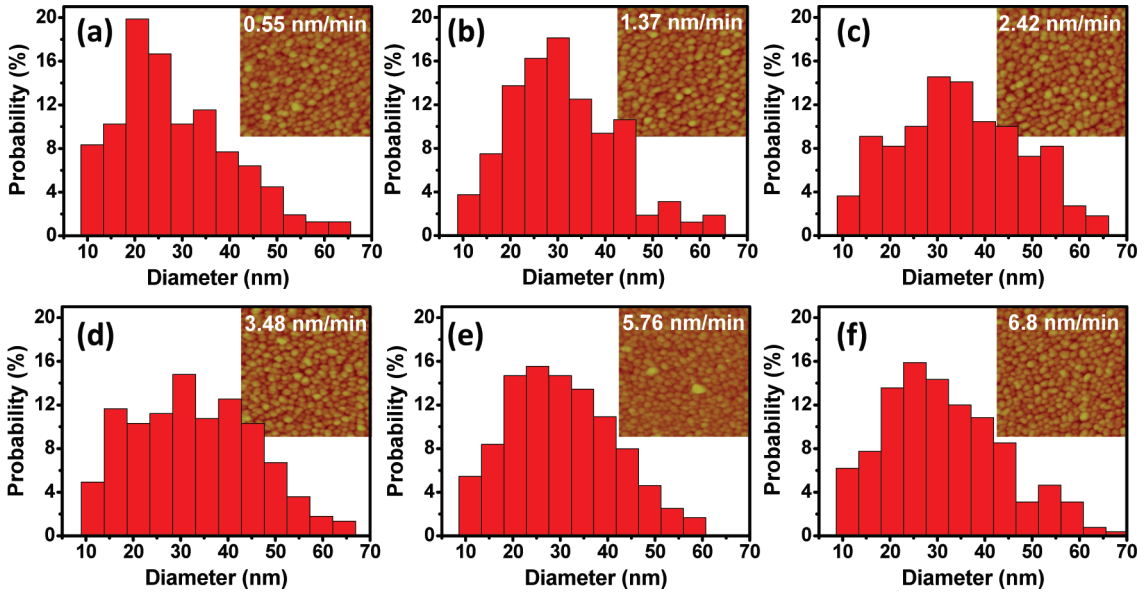

Figure 1. (a–f) Histograms of the grain diameter on the film at different deposition rates. Insets show AFM images at 1 × 1 μm for the corresponding rate.

Figure 1b–d). With even higher deposition rates, big grains (35 ± 10 nm) dominate (see Figure 1e,f).

As a further investigation, Figure 2a shows the surface roughness and mean diameter as a function of the deposition rate. It is observed first that the average diameter corresponds closely to the highest probability of the grain size formed, especially for low deposition rates. Second, on average, the grain size initially increases with the deposition rate and then fluctuates around 32 nm as the deposition rate is increased above 2.42 nm/min. This indicates that there is a limit to which the grains can grow. In addition, the surface roughness increases almost linearly with higher deposition rate (see the dotted fitting line in Figure 2a). Furthermore, Figure 2b shows the mean area (A) and count of the grains (i.e., number of particles, N, per 1 μm^2) as a function of the deposition rate. On this basis, the mean interparticle spacing = $(1\ \mu m^2 - AN)/N$, i.e., the gap between the particles, is plotted in the inset of Figure 2b. It is observed from both figures that variation of the deposition rate from 0.55 to 6.8 nm/min results in three different regions. The first region is before the first dotted line at rate ~2.42 nm/min, where the stacking of Ag atoms to form bigger grains dominates during deposition. In the second region, the Ag atoms are more mobile and the rate at which the Ag atoms hit on the substrate is now faster. It is easier for Ag atoms to move and congregate to each other to form a rougher film. There is also a tendency for the Ag atoms to diffuse along the island edge to form closer and smaller grains (see the histograms in Figure 1c–e).[28] In the third region, stacking continues, and at the same time, there are also Ag grains that are more mobile and can diffuse to coalesce with neighboring Ag grains. Thus, the grains may increase in size slightly. It is expected that at much higher rates (i.e., Ag atoms gain even larger mobility) and for longer deposition times (i.e., thicker film), semicontinuous films that consist of long islands instead of small individual grains (i.e., as a result of nucleation and coalescence) will be obtained as reported in most papers where the deposition rate is often >6 nm/min and the thickness >100 nm.[29]

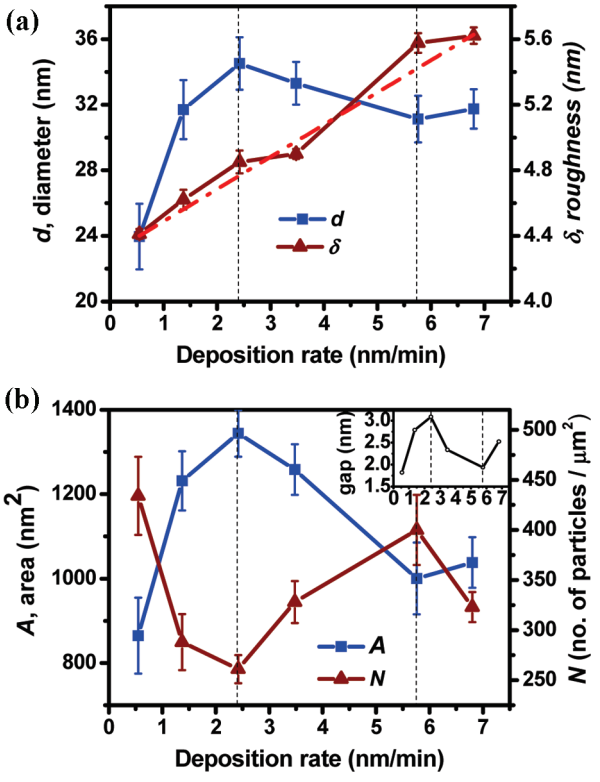

Figure 2. (a) Plot of the grain diameter, d, and the surface roughness of a multilayered film, δ, against the deposition rate (nm/min). The dash-dotted line shows a linear relationship between δ and the rate. (b) Plot of the grain area, A, and the number of particles, N, against the deposition rate. The inset shows the calculated interparticle spacing (gap) of the grains at different rates.

It is well-known that nonradiative surface plasmons on a rough metallic surface can be excited using normally incident light.[1] In order to investigate how the roughness affects the excitation of

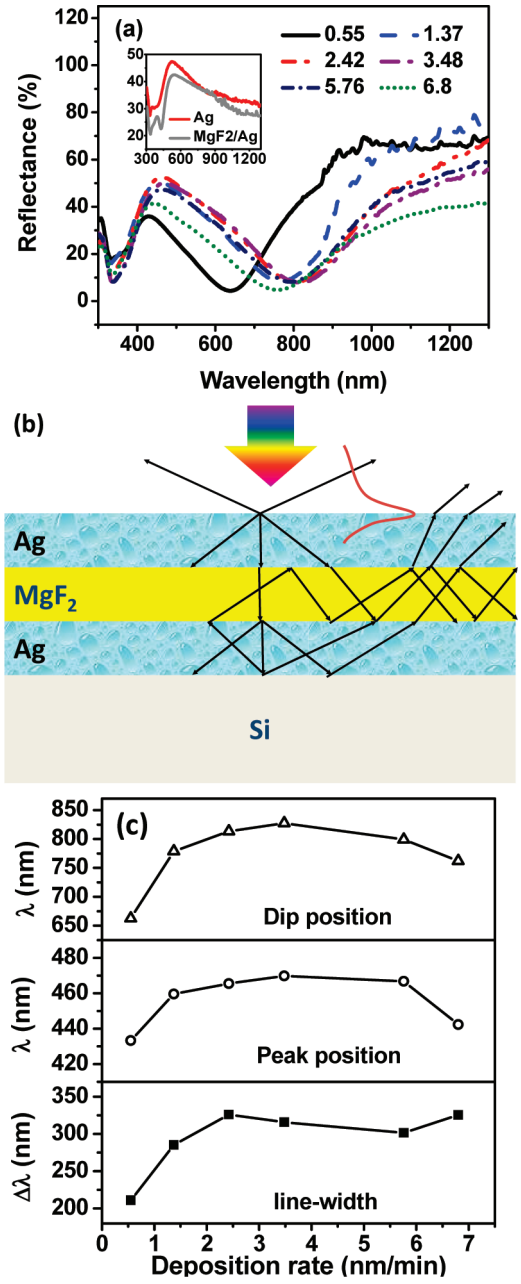

Figure 3. (a) Plot of different reflectance spectra for samples at different deposition rates. The inset shows the reflectance spectrum for a single Ag film and a MgF_2/Ag film on a Si substrate. (b) Schematic of the excitation of SPPs at the air/Ag interface that decays to the MgF_2 layer and gets reflected by the bottom Ag layer. (c) Extraction of the dip and peak positions and line width of the dip from part a plotted against the deposition rate.

surface plasmons, reflectance measurement was carried out using a UV−vis−near-IR microspectrophotometer (CRAIC QDI 2010). A 75 W Xe lamp was used as the source, and light was focused to a spot on the sample using a 36× microscope objective lens. The collection area was 7.1 × 7.1 μm^2. A Si substrate was used as the reference material for all measurements. The inset in Figure 3a shows the reflectance spectrum for a 30-nm-thick Ag film on Si and MgF_2 (30 nm)/Ag (30 nm)/Si. Reflectance peaks at ∼526 and 539 nm are observed for the Ag and MgF_2/Ag films, respectively. These peaks come from the film discontinuity, and the scattering of light comes from the random Ag grains.[30] For a smoother and smaller grain Ag film, formed either with a Ge seed layer or a fast deposition rate with a thicker film,[16−18] a high reflectivity over the 400−1200 nm range will be observed. The presence of a reflectance dip at ∼340 nm is due to the interband transitions from the d bands to the conduction state, which is around 3.5−3.8 eV.[14,31,32] Figure 3a shows the reflectance spectra of the Ag/MgF_2/Ag films at different deposition rates. An additional reflectance dip in the range of 650−800 nm, aside from the UV dip, is observed. The position of the dip depends on the deposition rate. We believe that this is due to the coupling of light to the SPPs at the air/Ag interface, and the peak-to-dip intensity is an indication of the efficiency of SPP excitation. The top rough grainy Ag surface scatters some of the light and also alters the wave vector of the light such that light of higher wave vector can be coupled into SPPs at the air/Ag interface. Because the top semicontinuous Ag film is quite thin (only ∼30 nm), the SPPs can tunnel through the thin Ag film and leak into the MgF_2 layer. A certain amount of light is coupled into the waveguide mode in the MgF_2 layer between the two Ag films, as shown in the schematic in Figure 3b. The arrows indicate the possible paths that light may travel after hitting upon the top rough Ag surface. Furthermore, because of the rough Ag/MgF_2 interface, some light can still escape to the top Ag layer and couple into the SPPs again at the air/Ag interface, thus repeating the above-mentioned process. It is noted that, if the bottom Ag film is absent, a dip in the visible range still exists because the SPPs at the air/Ag interface can still be excited via the above-proposed mechanism (i.e., Si reflects the light, in place of the bottom Ag layer). However, in the absence of the top Ag film (i.e., MgF_2/Ag/Si), the smoother MgF_2 film could not change the wave vector of light to excite the SPPs at the MgF_2/Ag interface. On the other hand, for Ag/Si, any excited SPPs just leak into the substrate. Hence, the dip in the visible range cannot be observed.

A more detailed analysis of the reflectance spectrum is presented in Figure 3c. In general, a dip at a shorter wavelength has a smaller peak-to-dip intensity because of higher ohmic loss in the metal. Both the peak and dip positions vary in a similar fashion for different deposition rates. The change in the peak position (∼40 nm) is much smaller compared to that of the dip position (∼150 nm). This is reasonable because the peak indicates the color of light that is reflected and should not vary too much for the same thickness of deposited films.[30] Moreover, the mean grain diameter and interparticle spacing do not vary too much for the six samples. In addition, the line width of the dip first increases and then saturates at around 320 nm with higher deposition rates. The line width of the dip can be qualitatively linked to the amount of SPPs leaked and confined in the MgF_2 layer as a result of the surface roughness. This indicates the scattering strength of light and could be attributed to losses of SPPs caused by the surface-roughness-induced scattering[17] and scattering between the grains.[33,34] Typically, a rougher surface and/or larger particles increase the scattering strength and broaden the line width of the dip.

The visible dip in the reflectance spectrum of the MDM structure can be further understood through simulation of its reflectance. We used the Drude−Lorentz function for our Ag film and parameters similar to those shown in refs 18 and 35.

$$\varepsilon_{Ag}(\omega) = \varepsilon_1 - \frac{{\omega_p}^2}{\omega^2 + i\gamma_p\omega} + \sum_{m=1}^{5} \frac{f_m {\omega_m}^2}{{\omega_m}^2 - \omega^2 - i\gamma_m\omega}$$

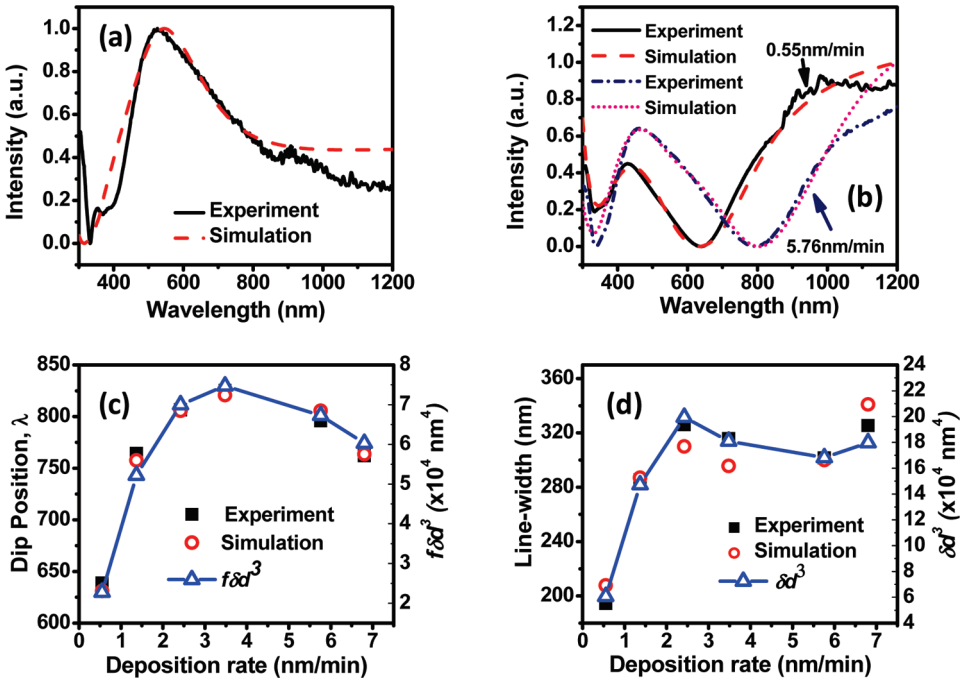

Figure 4. Comparison of the measured and simulated reflectance curves for (a) a single Ag layer and (b) MDM layers deposited at 0.55 and 5.76 nm/min. Comparison of the measured and simulated (c) dip position and (d) line width of the visible dip. Empirical fits between the optical spectra and AFM data are also shown in parts c and d.

In these parameters, ε_1 describes the contribution of electrons from the d band to the conduction band[14,31,32] and varies in our samples. The damping rate γ_p is also affected by the scattering of electrons due to defects and grain boundaries,[18,35,36] and it is linearly proportional to $1/r$, where r is the radius of the particle. For a discontinuous film with a low filling ratio, f, besides the above surface dispersion effect, the filling ratio also played an important role in influencing the optical properties.[18,34,37] From the Maxwell−Garnett theory, the effective permittivity, $\varepsilon(\omega)$, of the Ag film is given by

$$\frac{\varepsilon(\omega)-\varepsilon_d(\omega)}{\varepsilon(\omega)+2\varepsilon_d(\omega)} = f\frac{\varepsilon_{Ag}(\omega)-\varepsilon_d(\omega)}{\varepsilon_{Ag}(\omega)+2\varepsilon_d(\omega)}$$

where $\varepsilon_d(\omega)$ is the permittivity of the dielectric medium. From the AFM data, we can estimate the filling ratio, f, to be the number of particles in 1 μm^2 of the AFM image times the average area of each particle, which is equivalent to $NA/(1\ \mu m^2)$. The refractive index of MgF_2 follows a Lorentz−Lorentz formula, as listed in ref 38.

In our simulation, we considered the bottom Ag film and most of the top Ag layer to be in contact with MgF_2, while a thin top Ag layer is also in contact with air. The thickness of the Ag film in contact with air is approximated by the surface roughness of the film. We adopted the Fresnel matrix formalization to calculate the reflectance of the multilayered films. At a normal incidence angle, the characteristic matrix for each p layer is given by[39]

$$M_p = \begin{bmatrix} \cos\left(\frac{2\pi n_p d_p}{\lambda_0}\right) & -\frac{i}{g_p}\sin\left(\frac{2\pi n_p d_p}{\lambda_0}\right) \\ -ig_p \sin\left(\frac{2\pi n_p d_p}{\lambda_0}\right) & \cos\left(\frac{2\pi n_p d_p}{\lambda_0}\right) \end{bmatrix}$$

where $g_p = (\varepsilon_0/\mu_0)^{1/2} n_p$ for s polarization ($\perp$) and $g_p = (\mu_0/\varepsilon_0)^{1/2}(1/n_p)$ for p polarization ($\parallel$).

Thus, the characteristic matrix $\mathbf{M}$ of this thin film system is given by

$$\mathbf{M} = M_{eff\_Ag\_air} \cdot M_{eff\_Ag\_MgF_2} \cdot M_{MgF_2} \cdot M_{Ag\_MgF_2} = \begin{bmatrix} m_{11} & m_{12} \\ m_{21} & m_{21} \end{bmatrix}$$

where $M_{eff\_Ag\_air}$ represents the top layer of Ag in contact with air, $M_{eff\_Ag\_MgF_2}$ represents the top layer of Ag in contact with MgF_2, M_{MgF_2} represents the MgF_2 layer, and $M_{Ag\_MgF_2}$ represents the bottom Ag layer that is in contact with MgF_2.

The reflection coefficient, $r_{\perp,\parallel}$, can then be calculated by the equation below, which takes into account the substrate and air:

$$r_{\perp,\parallel} = \frac{g_{air}(m_{11}+g_{substrate}m_{12}) - g_{air}(m_{21}+g_{substrate}m_{22})}{g_{air}(m_{11}+g_{substrate}m_{12}) + g_{air}(m_{21}+g_{substrate}m_{22})}$$

The reflectance is given by $R_{\perp,\parallel} = |r_{\perp,\parallel}|^2$. For unpolarized light, the reflectance is $R_0 = (1/2)(R_\perp + R_\parallel)$. Taking a step further to consider the surface roughness effect on the specular reflectance at normal incidence, we finally get the reflectance[40,41]

$$R = R_0 \exp\left[-\left(\frac{4\pi\delta}{\lambda}\right)^2\right]$$

In our experiment, the bottom Ag layer is deposited at the same time for all samples. Therefore, the effective permittivity of the bottom Ag layer should be the same. Thus, we first try to fit the single Ag layer reflectance curve, and the result is presented in Figure 4a. The fitting parameters are $\varepsilon_{1,bottom} = 5.5$, $\gamma_{p,bottom} = 0.55$ eV, and $d_{Ag} = 30$ nm. A reasonable match has been obtained.

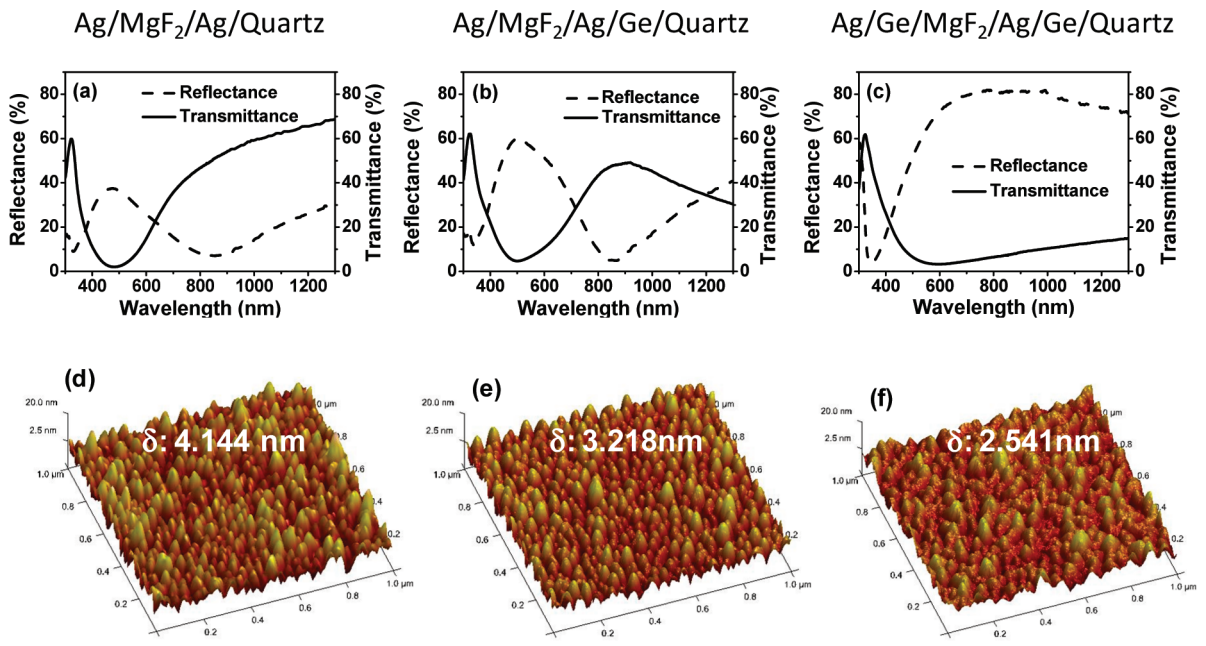

Figure 5. Reflectance and transmittance spectra for (a) $Ag/MgF_2/Ag$, (b) $Ag/MgF_2/Ag/Ge$, and (c) $Ag/Ge/MgF_2/Ag/Ge$ on quartz. The corresponding AFM images are shown in parts d−f.

Figure 4b shows the experimental and simulated reflectance spectra for two sets of films deposited at 0.55 and 5.76 nm/min deposition rates, respectively. In the simulation of the $Ag/MgF_2/Ag$ film, we fixed the permittivity and thickness of the bottom Ag layer and used the experimental data (i.e., δ and f) from AFM analysis. The fitting parameters for the top Ag layer used are as follows: $\varepsilon_{1,top} = 1.5 \pm 0.5$ eV, $\gamma_{p,top} = 1.52 \pm 0.53$ eV, $d_{Ag,top} = 31 \pm 2$ nm, and $d_{MgF_2} = 31 \pm 2$ nm. It is worth mentioning that similar fittings are also achieved for other sets of data at different deposition rates. We found that a higher filling factor f red-shifts the dip position. To a smaller extent, a larger surface roughness red-shifts the dip position, and the overall scattering and size effects on γ_p also play a role in determining the dip position (i.e., a smaller γ_p red-shifts the visible dip position). On the contrary, ε_1 affects only the position of the UV dip and does not affect that of the visible dip. For the line width of the visible dip, the size of the particle has a big effect. In general, a smaller particle size results in larger γ_p. Thus, the amount of light scattering is less, and the line width of the visible dip is small. On the other hand, a larger surface roughness at a higher deposition rate exposes more Ag particles in contact with air, and this also increases the scattering of light and hence gives a larger line width. We also attempted to do an empirical fit of the optical data with the morphology information and found the relationships of $\lambda \sim f\delta d^3$ and line width $\sim \delta d^3$, as shown in Figure 4c,d. This agrees well with the above discussion that both the dip position and line width are affected by the particle size and surface roughness and that the dip position is also affected by the filling ratio.

We also plotted the experimental and simulated dip positions and their line widths for different deposition rates in parts c and d of Figure 4, respectively. The simulated data fit quite well with the experimental data for the dip position, while there is a slight mismatch in the line width of the visible dip at higher deposition rates. This could be because we did not take into account the particle-induced scattering effect in the above analysis. At higher deposition rates, the film becomes rougher and the particles become bigger (>30 nm). As discussed by Noguez in refs 34 and 42, radiation damping effects ($\propto r^3$) become important for particles larger than 30 nm in diameter. This can result in broader and less intense surface plasmon resonances. Furthermore, we may need to consider the depolarization field in the permittivity equation, as listed in refs 37 and 43, because the Ag grains are not exactly spherical. The effect of the depolarization field would be to red-shift the spectrum.[34,42] A more in-depth study is required to see how this will affect the MDM structure.

As a control experiment, we repeated deposition of the MDM structure on a quartz substrate and measured its transmittance, reflectance, and surface roughness. The deposition rate of the top and bottom Ag films was 6 nm/min, while that of the MgF_2 film was 1.5 nm/min. Figure 5a shows the transmittance and reflectance spectra. There exists a dip at ~500 nm in the transmittance spectrum, which corresponds to the reflectance peak (i.e., due to scattering of light by Ag grains). However, the transmittance peak corresponding to the reflectance dip is not observed. A possible reason could be that the leakage light tunnels through the rough bottom Ag layer and escapes from the quartz substrate. The measured surface roughness δ is ~4.144 nm from the AFM image (Figure 5d). It is noted that the surface roughness of the Ag film on quartz tends to be smaller than that on Si. To improve the confinement, an attempt to smoothen the Ag layer was carried out. This can be achieved by depositing a 1 nm Ge seed layer prior to deposition of the Ag layer.[16,17] Figure 5b shows the optical spectra for the $Ag/MgF_2/Ag/Ge$/quartz configuration. The corresponding AFM image in Figure 5e shows that the surface morphology is similar except that the smoothness of the film is improved (δ = 3.218 nm). The bottom Ag layer is now more reflective. Furthermore, the smoother interface between the bottom Ag layer and the MgF_2 layer will reduce the scattering loss. Therefore, both of these effects collectively improve the confinement of light in the MgF_2 layer, thus contributing to an increase in the peak-to-dip intensity. As such, a transmittance peak at ~800 nm was observed. Through control of the

deposition rate of the top Ag layer, transmittance peaks at different wavelength regions can be obtained. This could be an effective way to design plasmonic thin film color filters.[22] As another control experiment, a Ag/Ge/MgF_2/Ag/Ge/quartz sample was also prepared and tested, as shown in Figure 5c. The surface roughness has been greatly improved, and grains are smaller. The interparticle spacing is also bigger, as shown in Figure 5f. These factors may reduce the scattering efficiency of light, and SPPs cannot be excited at the Ag/air interface. Therefore, the reflectance and transmittance spectra resemble that of bulk Ag on quartz.

CONCLUSIONS

We have studied the surface morphology of Ag/MgF_2/Ag films and their corresponding reflectance spectra. A dip in the visible range of the reflectance spectrum is found to shift with different Ag surface properties. We proposed that SPP excitation at the air/Ag interface due to the surface roughness is the main reason for the reflectance dip. Through the theoretical fitting of the experimental data, we found that the filling ratio of the Ag film plays an important role in determining the dip position, while for the line width, scattering due to the particle size and surface roughness is the main contribution. Furthermore, the application of this MDM structure was explored. The unique feature made this thin film system promising for color filters. Studies of such a MDM structure will be potentially useful in the design of plasmonic devices and metamaterial structures.

AUTHOR INFORMATION

Corresponding Author
*E-mail: jh-teng@imre.a-star.edu.sg.

ACKNOWLEDGMENT

This work was financially supported by A*STAR under Grants 092 1540099, 092 1540098, and 092 1450030.

REFERENCES

(1) Raether, H. *Surface plasmons on smooth and rough surfaces and on grating*, 1st ed.; Springer-Verlag: Berlin, 1986; Chapters 3−5.
(2) Chen, J.; Smolyakov, G. A.; Brueck, S. R. J.; Malloy, K. J. *Opt. Express* **2008**, *16*, 14902–14909.
(3) Dionne, J. A.; Sweatlock, L. A.; Atwater, H. A.; Polman, A. *Phys. Rev. B: Condens. Matter Mater. Phys.* **2006**, *73*, 035407.
(4) Liu, Y. J.; Hao, Q. Z.; Smalley, J. S. T.; Liou, J.; Khoo, I. C.; Huang, T. J. *Appl. Phys. Lett.* **2010**, *97*, 091101.
(5) Zhang, X.; Liu, Z. W. *Nat. Mater.* **2008**, *7*, 435–441.
(6) Srituravanich, W.; Pan, L.; Wang, Y.; Sun, C.; Bogy, D. B.; Zhang, X. *Nat. Nanotechnol.* **2008**, *3*, 733–737.
(7) Chaturvedi, P.; Wu, W.; Logeeswaran, V. J.; Yu, Z. N.; Saif Islam, M.; Wang, S. Y.; Stanley Williams, R.; Fang, N. X. *Appl. Phys. Lett.* **2010**, *96*, 043102.
(8) Bergman, D. J.; Stockman, M. I. *Phys. Rev. Lett.* **2003**, *90*, 027402.
(9) Seidel, J.; Grafstrom, S.; Eng, L. *Phys. Rev. Lett.* **2005**, *94*, 177401.
(10) Noginov, M. A.; Zhu, G.; Mayy, M.; Ritzo, B. A.; Noginova, N.; Podolskiy, V. A. *Phys. Rev. Lett.* **2008**, *101*, 226806.
(11) Zheludev, N. I.; Prosvirnin, S. L.; Papasimakis, N.; Fedotov, V. A. *Nat. Photonics* **2008**, *2*, 351–354.
(12) Liu, N.; Fu, L. W.; Kaiser, S.; Schweizer, H.; Giessen, H. *Adv. Mater.* **2008**, *20*, 3859–3865.
(13) Li, T.; Liu, H.; Wang, F. M.; Li, J. Q.; Zhu, Y. Y.; Zhu, S. N. *Phys. Rev. E: Stat., Nonlinear, Soft Matter Phys.* **2007**, *76*, 016606.
(14) Wang, Z. G.; Cai, X.; Chen, Q. L.; Li, L. H. *Vacuum* **2006**, *80*, 438–443.
(15) Zhang, S.; Berguiga, L.; Elezgaray, J.; Roland, T.; Faivre-Moskalenko, C.; Argoul, F. *Surf. Sci.* **2007**, *601*, 5445–5458.
(16) Logeeswaran, V. J.; Kobayashi, N. P.; Islam, M. S.; Wu, W.; Chaturvedi, P.; Fang, N. X.; Wang, S. Y.; Williams, R. S. *Nano Lett.* **2009**, *9*, 178–182.
(17) Liu, H.; Wang, B.; Leong, E. S. P.; Yang, P.; Zong, Y.; Si, G. Y.; Teng, J. H.; Maier, S. A. *ACS Nano* **2010**, *4*, 3139–3146.
(18) Chen, W. Q.; Thoreson, M. D.; Ishii, S.; Kildishev, A. V.; Shalaev, V. M. *Opt. Express* **2010**, *18*, 5124–5134.
(19) Mills, D. L.; Maradudin, A. A. *Phys. Rev. B: Condens. Matter Mater. Phys.* **1975**, *12*, 2943–2958.
(20) Hoffmann, A.; Lenkefi, Z.; Szentirmay, Z. *J. Phys.: Condens. Matter* **1998**, *10*, 5503–5513.
(21) Kolomenski, A.; Kolomenskii, A.; Noel, J.; Peng, S.; Schuessler, H. *Appl. Opt.* **2009**, *48*, 5683–5691.
(22) Jakšić, Z.; Maksimović, M.; Sarajlić, M.; Tanasković, D. *Acta Phys. Pol., A* **2007**, *112*, 953–958.
(23) Crego, C. R.; Rustgi, M. L. *J. Opt. Soc. Am. B* **1990**, *7*, 877–884.
(24) Watanabe, J.; Uehara, Y.; Ushioda, S. *Phys. Rev. B: Condens. Matter Mater. Phys.* **1995**, *52*, 2860–2867.
(25) Hayashi, S.; Kamada, Y.; Maekeawa, A.; Fujii, M.; Hayashi, S. *J. Lumin.* **2009**, *129*, 1997–1999.
(26) Brumfiel, G. *Nature* **2009**, *459*, 504–505.
(27) Min, C.; Veronis, G. *Opt. Express* **2010**, *18*, 20939–20948.
(28) Ratsch, C.; Venables, J. A. J. *Vac. Sci. Technol., A* **2003**, *21*, S96–S109.
(29) Kaspar, W.; Kreibig, U. *Surf. Sci.* **1977**, *69*, 619–636.
(30) Gupta, R.; Dyer, M. J.; Weimer, W. A. *J. Appl. Phys.* **2002**, *92*, 5264–5271.
(31) Pinchuk, A.; Kreibig, U.; Hilger, A. *Surf. Sci.* **2004**, *557*, 269–280.
(32) He, Y.; Zeng, T. *J. Phys. Chem. C* **2010**, *114*, 18023–18030.
(33) Catchpole, K. R.; Polman, A. *Opt. Express* **2008**, *16*, 21793–21800.
(34) Zhang, J. Z.; Noguez, C. *Plasmonics* **2008**, *3*, 127–150.
(35) Drachev, V. P.; Chettiar, U. K.; Kildishev, A. V.; Yuan, H. K.; Cai, W. S.; Shalaev, V. M. *Opt. Express* **2008**, *16*, 1186–1195.
(36) Hövel, H.; Fritz, S.; Hilger, A.; Kreibig, U.; Vollmer, M. *Phys. Rev. B: Condens. Matter Mater. Phys.* **1993**, *48*, 18178.
(37) Dalacu, D.; Martinu, L. *J. Opt. Soc. Am. B* **2001**, *18*, 85–92.
(38) https://www.cvimellesgriot.net/Products/Documents/Technical-Guide/Optical-Coatings.pdf.
(39) Kuhn, K. J. *Laser Engineering*, 1st ed.; Prentice-Hall, Inc.: New York, 1998; Chapter 8.2.1.
(40) Hunderi, O. *Surf. Sci.* **1980**, *96*, 1–31.
(41) Bennett, H. E.; Porteus, J. O. *J. Opt. Soc. Am.* **1961**, *51*, 123–129.
(42) Noguez, C. *Opt. Mater.* **2005**, *27*, 1204–1211.
(43) Sihvola, A. *PIER* **2005**, *51*, 65–82.